

## Article

# Determination of Dipicolinic Acid through the Antenna Effect of Eu(III) Coordination Polymer

Jing Li <sup>1,2,†</sup>, Yu Liang <sup>2,3,†</sup>, Chun Tian <sup>2</sup>, Hongyan Zou <sup>2</sup> , Lei Zhan <sup>2</sup>, Lijuan Wang <sup>1,\*</sup>, Chengzhi Huang <sup>2</sup> and Chunmei Li <sup>2,\*</sup> 

- <sup>1</sup> Department of Basic Medicine, Shangqiu Medical College, Shangqiu 476100, China; liching1028@163.com
- <sup>2</sup> Key Laboratory of Biomedical Analytics (Southwest University), Chongqing Science and Technology Bureau, College of Pharmaceutical Sciences, Southwest University, Chongqing 400715, China; 13637866124@163.com (Y.L.); tianchun2001@email.swu.edu.cn (C.T.); zhy2013@swu.edu.cn (H.Z.); zhanlei6@swu.edu.cn (L.Z.); chengzhi@swu.edu.cn (C.H.)
- <sup>3</sup> Environment and Quality Test Department, Chongqing Chemical Industry Vocational College, Chongqing 401228, China
- \* Correspondence: wlj.wang@163.com (L.W.); licm1024@swu.edu.cn (C.L.); Tel.: +86-2368254059 (C.L.); Fax: +86-2368367257 (C.L.)
- † These authors contributed equally to this work.

**Abstract:** *Bacillus anthracis* is a Gram-positive bacterium that can cause acute infection and anthrax, which is a serious concern for human health. Determining *Bacillus anthracis* through its spore biomarker dipicolinic acid (DPA) is crucial, and there is a strong need for a method that is rapid, sensitive, and selective. Here, we created Eu(III)-coordination polymers (Eu-CPs) with surfaces that have abundant carboxyl and hydroxyl groups. This was achieved by using citric acid and europium nitrate hexahydrate as precursors in a straightforward one-pot hydrothermal process. These Eu-CPs were then successfully utilized for highly sensitive DPA determination. The fluorescence (FL) emission of Eu-CPs, which is typically weak due to the coordination of Eu(III) with water molecules, was significantly enhanced in the presence of DPA. This enhancement is attributed to the competitive binding between DPA's carboxyl or hydroxyl groups and water molecules. As a result, the absorbed energy of DPA, when excited by 280 nm ultraviolet light, is transferred to Eu-CPs through an antenna effect. This leads to the emission of the characteristic red fluorescence of Eu<sup>3+</sup> at 618 nm. A strong linear relationship was observed between the enhanced FL intensity and DPA concentration in the range of 0.5–80 μM. This relationship allowed for a limit of detection (LOD) of 15.23 nM. Furthermore, the Eu-CPs we constructed can effectively monitor the release of DPA from *Bacillus subtilis* spores, thereby further demonstrating the potential significance of this strategy in the monitoring and management of anthrax risk. This highlights the novelty of this approach in practical applications, provides a valuable determination technique for *Bacillus anthracis*, and offers insights into the development cycle of microorganisms.

**Keywords:** Eu(III)-coordinated polymers (Eu-CPs); antenna effect; dipicolinic acid (DPA); biomarkers of *Bacillus anthracis* spores



**Citation:** Li, J.; Liang, Y.; Tian, C.; Zou, H.; Zhan, L.; Wang, L.; Huang, C.; Li, C. Determination of Dipicolinic Acid through the Antenna Effect of Eu(III) Coordination Polymer. *Molecules* **2024**, *29*, 4259. <https://doi.org/10.3390/molecules29174259>

Academic Editors: Michal Szostak and Graham Saunders

Received: 30 July 2024

Revised: 28 August 2024

Accepted: 5 September 2024

Published: 8 September 2024



**Copyright:** © 2024 by the authors. Licensee MDPI, Basel, Switzerland. This article is an open access article distributed under the terms and conditions of the Creative Commons Attribution (CC BY) license (<https://creativecommons.org/licenses/by/4.0/>).

## 1. Introduction

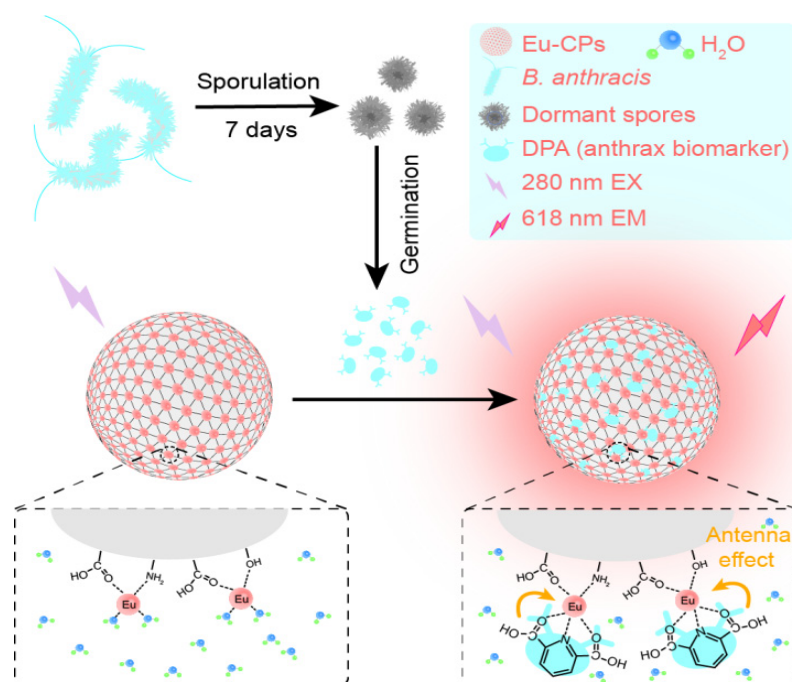
*Bacillus anthracis* is a Gram-positive bacterium responsible for causing anthrax [1]. Anthrax primarily affects herbivores and is typically the result of natural infection. Humans usually become infected with anthrax through contact with infected animals or contaminated animal products [2]. Due to the high pathogenicity, lethality, and infectivity of *Bacillus anthracis*, the potential use of anthrax spores as a biological weapon by bioterrorists is a significant concern [3]. Consequently, there is a pressing need for accurate, rapid, and sensitive methods for the detection of *Bacillus anthracis*. This bacterium exhibits remarkable resilience; when environmental conditions are unfavorable for growth—such as

exposure to high temperatures, high pressure, or ultraviolet light—it can enter a dormant state and produce spores [4]. When the growth environment is optimal, the spores germinate and release a variety of substances. Plasmids, such as pXO1 and pXO2, are frequently used as *Bacillus anthracis* nucleic acid determination targets. Some specific chromosomal sequences, such as *BA813*, *RpoB*, and *Gyra*, have been identified as biomarkers thanks to advances in genomics. For example, anthrax toxin is made up of three components: protective antigen (PA) [5], lethal factor (LF) [6], and edema factor (EF) [7]. PA and LF combine to form a lethal toxin, while a combination of PA and EF produces edema toxin. These toxin components are critical for determining *Bacillus anthracis* and diagnosing anthracnose. For instance, 2,6-dipicolinic acid (DPA), the main component of spores, contributes significantly to spore resistance and can be used as a *Bacillus anthracis* biomarker [8,9]. Although *BA813*, *RpoB*, *Gyra*, or PA, LF, EF, and other biomarkers can be chosen for their high accuracy and sensitivity in determining anthrax spores, the sample pretreatment and extraction processes are time-consuming and labor-intensive, require expensive equipment, etc., and result in a relatively high cost and difficult operation [10]. Therefore, we have selected DPA as an anthrax spore biomarker. In the field of DPA analysis, the primary clinical strategy for detecting anthrax involves evaluating genetic sequences and employing polymerase chain reaction (PCR) and enzyme-linked immunosorbent assay (ELISA) techniques. PCR amplifies specific DNA sequences associated with diphtheria toxin production, while ELISA utilizes specific antibodies to detect and quantify diphtheria toxin levels [10,11]. Unfortunately, the prolonged detection process for anthrax spores not only delays the rapid identification of the disease but also heightens the risk of infection. The fluorescence spectroscopy is used to detect the target quickly, sensitively, and accurately without the need for complicated operation methods, expensive instruments, and equipment [12–17].

Lanthanide ions ( $\text{Ln}^{3+}$ ) have low luminescence efficiency under UV/Vis illumination due to their small molar absorption coefficient and forbidden f-f transition [18]. However, it is classified as a Lewis acid because it has a high affinity for bonding with negatively charged, neutral oxygen or nitrogen atoms [19]. Because of these physicochemical properties, it can bind to the site of the corresponding small organic molecules, known as “antenna ligands”, that can participate in the energy transfer process, resulting in interesting photoluminescence properties [20]. This process, like large Stokes shifts and linear emission spectral bands, is known as the “antenna effect”. In addition, among other strong luminescent ions, such as  $\text{Sm}^{3+}$ ,  $\text{Tb}^{3+}$ , and  $\text{Dy}^{3+}$ ,  $\text{Eu}^{3+}$  has a longer emission wavelength, making it widely used [21–26].

In this work, Eu(III)-coordinated polymers (Eu-CPs) with rich surface carboxyl and hydroxyl groups were first prepared by using citric acid and europium nitrate hexahydrate as precursors through a one-pot hydrothermal route. The synthesized Eu-CPs exhibit a low background signal, which can be attributed to the selection of ligand during material synthesis. In this context, citric acid was chosen as the ligand for several reasons: first, citric acid is abundant in carboxyl groups, and its oxygen atoms can effectively coordinate with  $\text{Eu}^{3+}$  ions; second, citric acid demonstrates greater water solubility compared to nitrogen-containing ligands; and third, citric acid occupies a portion of the coordination bonds of  $\text{Eu}^{3+}$ , preventing it from sensitizing  $\text{Eu}^{3+}$  to luminescence on its own. Furthermore, the remaining coordination sites of the Eu-CPs will be occupied by water molecules from the surrounding medium, which will further diminish the background fluorescence. Upon the introduction of the *Bacillus anthracis* spore biomarker DPA, it competes with the water molecules bound to the Eu-CPs for ligand binding, leading to the saturation of the  $\text{Eu}^{3+}$  ligand bonds. Concurrently, this competition inhibits the ability of water molecules to induce luminescence. Additionally, DPA absorbs energy from external 280 nm ultraviolet light, subsequently sensitizing the characteristic fluorescence emission of  $\text{Eu}^{3+}$  through the antenna effect, thereby facilitating the highly sensitive detection of DPA. The presence of DPA, one of the biomarkers of *Bacillus anthracis* spores, causes the Eu-CPs to have strong FL emission of  $\text{Eu}^{3+}$  owing to the antenna effect of Eu-CP DPA, achieving the goal of highly sensitive DPA determination. As a practical application, the number of *Bacillus*

*anthracis* spores was detected, and the DPA release process of *Bacillus anthracis* spores was monitored (Scheme 1), allowing for disease control and effective prevention of bacterial spore germination.



**Scheme 1.** Determination illustration of DPA, one of the biomarkers of *Bacillus anthracis* spores, through the “off-on” process of the antenna effect in Eu-CPs in the absence and presence of DPA. Arrows in the figure are used to indicate the sequence or flow between steps. The color change in the diagram of *Bacillus anthracis* represents the process of spore formation and germination.

## 2. Results and Discussion

### 2.1. Characteristic Features of Eu-CPs

As shown in Figure 1A, the as-prepared Eu-CPs displayed a typical spherical structure with an average particle size of  $1.16 \pm 0.14 \mu\text{m}$ , as determined by the scanning electron microscopic (SEM) image, which was consistent with the hydrodynamic diameter of  $1.22 \pm 0.0032 \mu\text{m}$  measured by dynamic light scattering (DLS), further confirming the consistency and uniformity of the Eu-CPs. Based on the analysis of the infrared spectrum, it can be observed that the  $\nu_{\text{C-H}}$  band [27] is associated with the absorption bands at  $2900.94$  and  $2827.64 \text{ cm}^{-1}$ . Additionally, the  $\nu_{\text{O-H}}$ ,  $\nu_{\text{C=O}}$ ,  $\nu_{\text{C-N}}$ , and  $\nu_{\text{C-O}}$  bands are denoted by the absorption bands at  $3406.29$ ,  $1577.77$ ,  $1419.61$ , and  $1080.14 \text{ cm}^{-1}$ , respectively [28]. Furthermore, the formation of the coordination bond between Eu and  $-\text{COOH}$  (or  $-\text{OH}$ ) was confirmed by the infrared absorption band at  $493.78 \text{ cm}^{-1}$  (Figure 1B) [29].

In addition, XPS spectra confirmed that the surface functional groups of Eu-CPs correspond to the infrared spectrum results. The three prominent peaks observed at  $288.6$ ,  $531.62$ , and  $1135.58 \text{ eV}$  were identified as C1s, O1s, and Eu3d, respectively (Figure 2C). The weaker peak at  $401.58 \text{ eV}$  was attributed to N1s. Three peaks at  $284.8$ ,  $286.4$ , and  $288.6 \text{ eV}$  were identified in the high-resolution XPS spectra of C1s; these peaks correspond to  $\text{C-C/C=C}$ ,  $\text{C-O}$ , and  $\text{C=O}$ , respectively (Figure S2A) [30].  $\text{C=O}$  and  $\text{C-OH}$  were identified as the two peaks at  $531.4$  and  $532.2 \text{ eV}$  in the O1s spectrum, respectively (Figure S2B) [27]. Two peaks at  $399.4$  and  $401.6 \text{ eV}$  in the N1s spectrum indicated the presence of minute quantities of  $\text{C-N}$  and  $\text{N-H}$ , respectively (Figure S2C) [31]. Two peaks at  $1125.5$  and  $1135.6 \text{ eV}$ , which correspond to  $\text{Eu(II)3d}^{5/2}$  and  $\text{Eu(III)3d}^{5/2}$  [32], respectively, were observed in the Eu3d spectrum (Figure S2D).

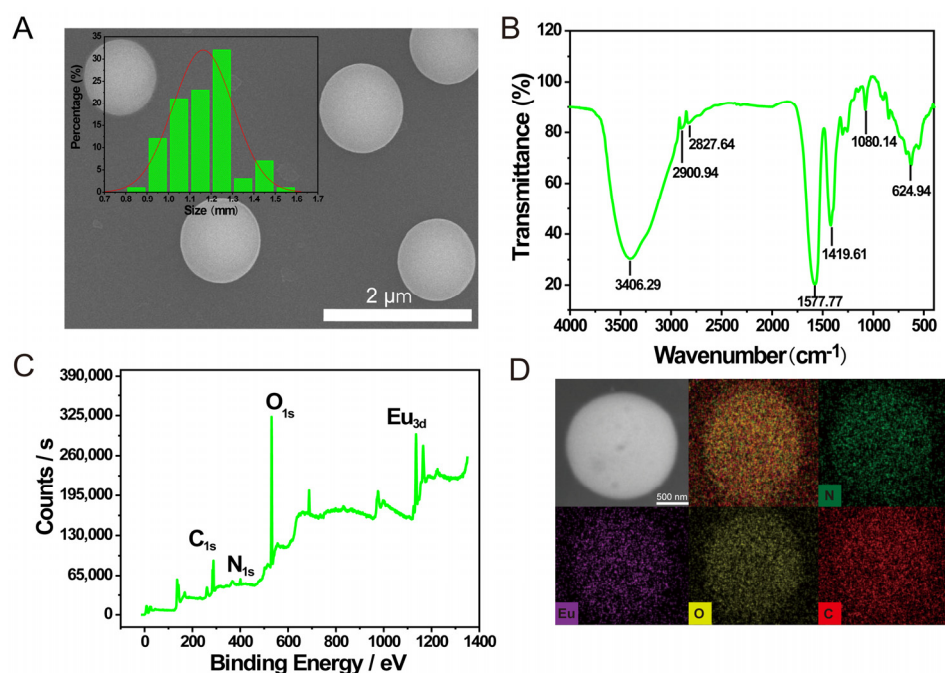


**Figure 1.** Characterization of Eu-CPs. (A) SEM image (inset: particle size distribution). (B) FT-IR spectrum. (C) XPS spectrum. (D) EDS mapping.

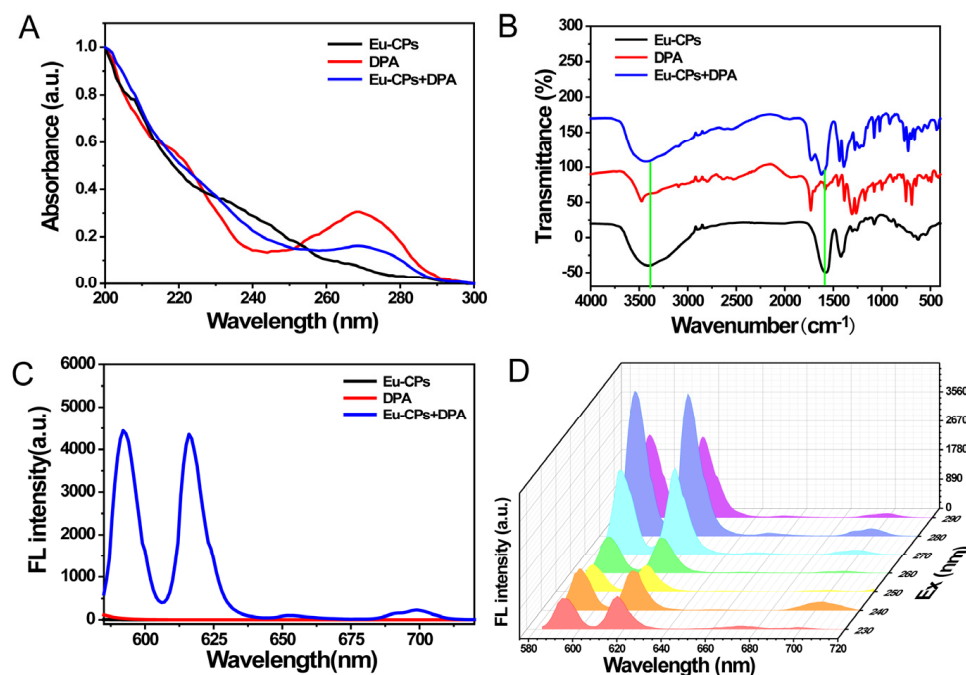


**Figure 2.** Optical properties of Eu-CPs after reacting with DPA. (A) UV absorption spectra of Eu-CPs, DPA, and Eu-CPs + DPA; (B) FT-IR spectra of Eu-CPs, DPA, and Eu-CPs + DPA. The green line marks the shift of infrared absorption peak; (C) fluorescence spectra of Eu-CPs, DPA, and Eu-CPs + DPA; (D) FL emission spectra of Eu-CPs + DPA under different excitation wavelengths from 230 to 290 nm. The line colors of the spectrum in the figure represent different excitation wavelengths.

The above results clearly demonstrated that the surface of Eu-CPs was covered in  $-\text{COOH}$ ,  $-\text{OH}$ , and  $-\text{NH}_2$  groups.  $\text{Eu}^{3+}$  was evenly distributed on the surface of Eu-CPs, as revealed by an energy-dispersive X-ray spectroscopy (EDS) mapping image (Figure 1D).

## 2.2. Investigation of the Reaction of Eu-CPs and DPA

Figure 2A illustrates that the synthesized Eu-CPs exhibit a weak absorption band due to their small molar absorption coefficient and forbidden f-f transition. Consequently, Eu-CPs demonstrate a significantly low luminous efficiency when exposed to ultraviolet light. By incorporating DPA as an antenna ligand [33], the absorption band of DPA in the 260–280 nm range decreased, indicating the formation of the Eu-CPs-DPA structure. This structure is capable of absorbing ultraviolet light energy and transferring it to Eu-CPs through an antenna effect. As a consequence,  $\text{Eu}^{3+}$  emits its characteristic FL.

In addition, the IR absorption bands at 3406.29 and 1577.77  $\text{cm}^{-1}$  of Eu-CPs exhibited a red shift after the addition of DPA, indicating the formation of a Eu-CPs-DPA structure through a coordination mechanism (Figure 2B) [34]. This result was further confirmed by fluorescence spectroscopy (Figure 2C). In addition, the emission of  $\text{Eu}^{3+}$  due to the antenna effect remained consistent regardless of the excitation wavelength, which ranged from 230 nm to 290 nm. The optimal excitation and emission wavelengths were found to be 280 nm and 618 nm, respectively (Figure 2D).

To achieve accurate analytical performance, we investigated the effect of environmental conditions such as acidity, salt, and light irradiation on the reaction stability of Eu-CPs and DPA. It was discovered that Eu-CPs, DPA, and Eu-CPs-DPA emit weak FL in acidic mediums because both carboxyl groups on the surface of Eu-CPs and DPA are protonated, and the coordination effect of DPA with Eu(III) is reduced, leading to reduced antenna effects and red FL [35]. The optimal pH condition was found to be 9.03 (Figure S3A). Exposing Eu-CPs to different concentrations of NaCl solution (40–200  $\mu\text{M}$ ) or an ultraviolet lamp for 7000 s had no significant effect on the fluorescence emission intensity with DPA (Figure S3B,C). The results showed that the newly formed Eu-CPs-DPA structure remained very stable despite changes in environmental conditions.

## 2.3. Analytical Performance of DPA

To investigate the analytical performance of the “fluorescence on” strategy for DPA determination under these ideal conditions, the fluorescence spectra of Eu-CPs with increasing DPA concentrations were measured. Figure 3A,B shows that FL intensity at 618 nm increased linearly with DPA concentration in the range of 0.5–80  $\mu\text{M}$ , following an equation of  $I - I_0 = 39.08c_{\text{DPA}} + 5.03$  with a correlation coefficient ( $R^2$ ) of 0.999. The LOD for DPA was 15.23 nM ( $3\sigma/k$ ) and the binding constant was  $3.32 \times 10^3 \text{ M}^{-1}$  (Figure S4), which is consistent with previously reported methods of DPA determination (Table S1).

Furthermore, this method has excellent selectivity and anti-interference capabilities. Figure 3C shows that only DPA causes an obvious increase in the FL emission of Eu-CPs in the presence of substances similar in structure to DPA, such as 2,4-dipicolinic acid (2,4-DPA), 2,5-dipicolinic acid (2,5-DPA), 3,4-dipicolinic acid (3,4-DPA), 3,5-dipicolinic acid (3,5-DPA), isonicotinic acid, phthalic acid, terephthalic acid, and isophthalic acid, even at concentrations nearly 7 times that of DPA. That is, Eu-CPs are highly selective and specific for DPA in aqueous solution. It should be noted that the presence of DPA in conjunction with other similar structural substances has no significant effect on the FL emission caused by the antenna effect (Figure 3D), demonstrating the excellent selectivity and anti-interference ability of the proposed method for DPA determination. We speculate that this selectivity is due to the unique molecular structure and electronic characteristics of DPA, which enable DPA to form a more stable coordination complex with Eu-CPs. Specifically, the spatial position of the two carboxyl groups of DPA may be more conducive to the effective coordination with the active sites on the surface of Eu-CPs [11,36].

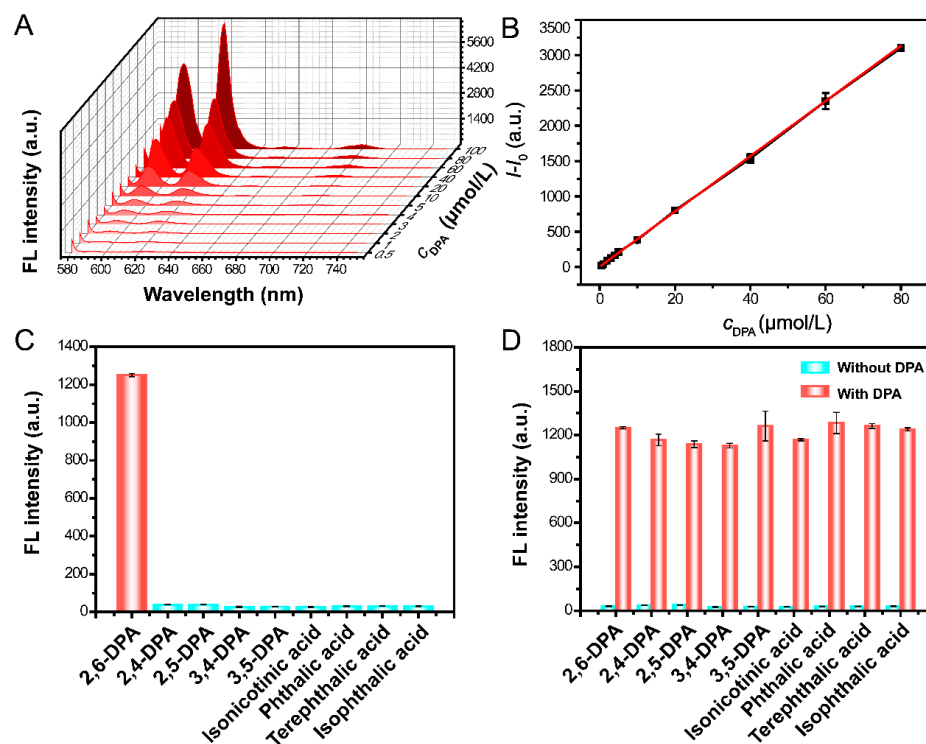


**Figure 3.** Fluorescence response, selectivity, and anti-interference of Eu-CPs for DPA determination. (A) The fluorescence intensity change of Eu-CPs with increasing DPA concentration. (B) Linear relationship between  $I - I_0$  and various DPA concentrations. (C) FL responses of Eu-CPs in the presence of 30  $\mu\text{M}$  DPA or 200  $\mu\text{M}$  of other interfering substances. Error bars represent standard deviations of three repetitive experiments ( $n = 3$ ). (D) FL responses of Eu-CPs in the coexistence of 30  $\mu\text{M}$  DPA and 200  $\mu\text{M}$  of other interfering substances. Error bars represent standard deviations of three repetitive experiments ( $n = 3$ ).

#### 2.4. Determination of the Bacterial Spores Amount

*Bacillus anthracis* is dormant and produces spores that initiate a self-protecting mechanism when exposed to high temperatures, high pressure, ultraviolet rays, etc. When the spores are in an environment favorable to their growth, they germinate and become pathogenic bacteria. Therefore, the quantitative evaluation of bacterial spores is extremely important [37]. For our experiments, we used *Bacillus subtilis* rather than the pathogenic *Bacillus anthracis*. To conduct spectral analysis, *Bacillus subtilis* suspension was diluted to various concentrations ( $1.4 \times 10^8$ ,  $2.8 \times 10^8$ ,  $4.2 \times 10^8$ ,  $5.6 \times 10^8$ , and  $8.2 \times 10^8$  spores  $\text{mL}^{-1}$ ) and lysed at 90 °C in dodecylamine for 1 h.

A modification in the emission signal at 618 nm was observed in each instance subsequent to the Eu-CPs treatment of the diluted suspensions. The emission intensity at 618 nm exhibits a progressive increase with the concentration of bacterial spores, as depicted in Figure 4A. A strong linear correlation was established between  $I - I_0$  and the spore concentration ( $I - I_0 = 322.10 \cdot c_{\text{Bacillus subtilis spores}} - 90.16$ ,  $R^2 = 0.999$ ) within the concentration range of  $1.4 \times 10^8$ – $8.2 \times 10^8$  spores  $\text{mL}^{-1}$  (Table S2, Figure S5A). The obtained LOD was calculated to be  $2.99 \times 10^7$  spores  $\text{mL}^{-1}$ . Due to the fact that every *Bacillus subtilis* spore contains  $3.65 \times 10^{-16}$  mols of DPA<sup>25</sup>, we were able to accurately determine the DPA concentration of various spore concentrations with relative errors ranging from  $-8.51\%$  to  $9.13\%$  (Table S2; Figure 4B). This suggests that the proposed method has the potential to be utilized for the quantitative evaluation of bacterial spores.

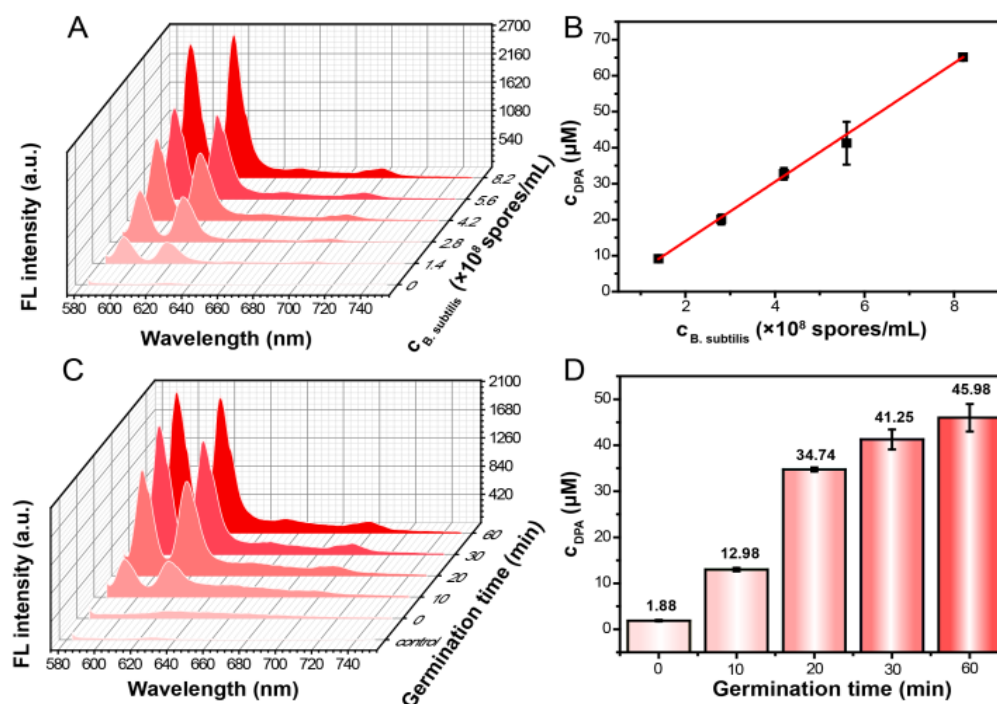


**Figure 4.** Study of biomarkers of *Bacillus anthracis* spores in actual samples by using Eu-CPs. (A) Fluorescence titration of Eu-CPs with different concentrations of *Bacillus subtilis* spore suspensions ( $1.4 \times 10^8$ ,  $2.8 \times 10^8$ ,  $4.2 \times 10^8$ ,  $5.6 \times 10^8$ , and  $8.2 \times 10^8$  spores  $\text{mL}^{-1}$ ) at pH 9.03 ( $\lambda_{\text{ex}} = 280$  nm, germination time = 2 h). (B) Linear relationship between  $c_{DPA}$  and  $c_{Bacillus subtilis}$  spores. (C) Fluorescence titration of Eu-CPs with different germination times (0, 10, 20, 30, and 60 min) of *Bacillus subtilis* suspensions at pH 9.03 ( $\lambda_{\text{ex}} = 280$  nm;  $c_{Bacillus subtilis}$  spores =  $6.18 \times 10^8$  spores  $\text{mL}^{-1}$ ). (D) Released amounts of DPA from *Bacillus subtilis* spores at different germination times. Error bars represent standard deviations of three repetitive experiments ( $n = 3$ ).

### 2.5. DPA Monitoring of the Germination of Bacterial Spores

To further demonstrate the practical applications of this method in actual biological scenarios, the researchers investigated the variation of DPA concentration released from *Bacillus subtilis* spores within 60 min using Eu-CPs. As shown in Figure 4C,D, as the germination time increased, the amount of DPA released from *Bacillus subtilis* spores increased gradually. Bacterial germination can be divided into three phases based on DPA release behavior. Figure 4D demonstrates that the first 20 min of rapid germination resulted in a DPA concentration of 34.74  $\mu$ M. *Bacillus subtilis* can grow quickly under these conditions. Therefore, *Bacillus subtilis* releases the majority of the DPA, which aids in spore germination. After 20 to 30 min, germination slowed, and DPA concentration reached 41.25  $\mu$ M. The release rate of DPA was slower in the final 30 to 60 min because most of the spores had completely germinated. The measured DPA concentration was 45.98  $\mu$ M, which was within 10% of the theoretical value of 45.11  $\mu$ M (calculated by releasing  $6.18 \times 10^8$  spores  $\text{mL}^{-1}$ ) (Figure S5B, Table S3). These observations provide useful information about the development cycles of microorganisms.

## 3. Experimental Section

### 3.1. Materials and Reagents

All chemicals used were at least analytical reagent grade and did not require any further purification. Europium nitrate hexahydrate ( $\text{Eu}(\text{NO}_3)_3 \cdot 6\text{H}_2\text{O}$ ) was purchased from Aladdin Chemistry Co., Ltd. in Shanghai, China. 2,6-Dipicolinic acid (DPA) and citric acid (CA) were commercially available from Merck Life Science Co., Ltd. (Shanghai, China); dodecylamine was purchased from Tokyo Chemical Industry Co., Ltd. (Tokyo, Japan); and

Britton–Robinson (BR) buffer was used to control acidity. The experiment utilized ultrapure water (18.2 M $\Omega$ ·cm, Mili-Q, Merck KgaA, Darmstadt, Germany).

### 3.2. Apparatus

The fluorescence (FL) spectra were obtained using an F-2500 spectrophotometer (Hitachi, Tokyo, Japan), with 5 nm slits for both excitation and emission and a photomultiplier tube (PMT) voltage of 700 V. The UV absorption spectra were measured using a Hitachi U-3010 spectrophotometer (Hitachi, Tokyo, Japan). An S-4800 SEM (Hitachi, Tokyo, Japan) was used to perform scanning electron microscopic characterizations. The infrared spectra were measured with an IR Prestige-21 instrument (Shimadzu, Tokyo, Japan). The elemental compositions were measured using an ESCALAB 250 X-ray photoelectron spectrometer (Thermo Fisher Scientific, Waltham, MA, USA). The FL lifetimes were measured using an FL-TCSPC FL spectrophotometer (Horiba Jobin Yvon, Stow, MA, USA). Hydrodynamic diameters were determined by Zetasizer Nano ZS (Malvern Instruments Ltd., Malvern, UK).

### 3.3. Synthesis of Eu-CPs

Eu-CPs were synthesized according to the procedure described in the literature [38]. Citric acid (874 mM) and Eu (NO<sub>3</sub>)<sub>3</sub> (200 mM) were synthesized using a hydrothermal method at 160 °C for 7 h in a Teflon-lined stainless steel autoclave. The reaction product was then allowed to cool naturally before being dialyzed for 72 h with a cellulose ester dialysis membrane (500 MWCO) to remove any residual raw material. Following dialysis, a white precipitate separated. By freeze-drying, a white powdery product of Eu-CPs was produced. In total, 5 mg of Eu-CPs was dispersed in 1 mL of ultrapure water. The mixture was sonicated for 2 min and then centrifuged at 8000 rpm for 5 min to obtain a supernatant containing 0.84 mg mL<sup>-1</sup> of the solution, which could be used for further processing.

### 3.4. FL Response of Eu-CPs to DPA

In a 1.5 mL tube, 200  $\mu$ L of Eu-CP supernatant (0.84 mg mL<sup>-1</sup>) and 400  $\mu$ L of BR buffer (pH 9.03) were added, followed by 200  $\mu$ L of DPA (concentrations ranging from 2.5 to 500  $\mu$ M). After thorough mixing, the solution was diluted to 1.0 mL with doubly distilled water and blended again. FL spectra were recorded immediately after mixing in the 560–700 nm range, with excitation at 280 nm.

### 3.5. Bacterial Spore Culture

Because both *Bacillus anthracis* and *Bacillus subtilis* have the same spore biomarker, dipicolinic acid (DPA), we chose *Bacillus subtilis* over the infectious *Bacillus anthracis* for the sake of safety. Bacterial cultivation was carried out using the previously described method [39]. For 7 days, third-generation *Bacillus subtilis* was cultured in LB liquid medium (10 mg mL<sup>-1</sup> tryptone, 5.0 mg mL<sup>-1</sup> yeast extract, 10 mg mL<sup>-1</sup> NaCl) at 37 °C and 200 rpm. After cultivation, the bacterial spore suspension was centrifuged at 6000 rpm for 10 min, washed 5 times with sterile water, diluted to 3.75  $\times$  10<sup>9</sup> spores mL<sup>-1</sup>, and stored at 4 °C in a refrigerator for future use.

### 3.6. DPA Determination during Spore Germination

To germinate and release DPA, a fresh suspension of *Bacillus subtilis* spores (1.4  $\times$  10<sup>8</sup> to 8.2  $\times$  10<sup>8</sup> spores mL<sup>-1</sup>) was diluted with sterile water and heated to 90 °C for 1 h with 0.66 mM of dodecylamine. Following that, the activated spore suspension was centrifuged at 10,000 rpm for 3 min to obtain the supernatant. Then, 100  $\mu$ L of the supernatant was added to a mixture containing 200  $\mu$ L of Eu-CPs (0.84 mg mL<sup>-1</sup>) and 400  $\mu$ L of BR buffer (pH 9.03), and the mixture was diluted to a final volume of 1 mL with ultrapure water. Immediately after mixing, the emission spectrum of the sample was recorded.

To activate the spores and release DPA, a fresh suspension of *Bacillus subtilis* was diluted to 6.18  $\times$  10<sup>8</sup> spores mL<sup>-1</sup> with sterile water and heated to 90 °C for different time



intervals (0, 10, 20, 30, and 60 min) with 0.66 mM of dodecylamine. The FL spectra were measured using the same procedure as described above.

#### 4. Conclusions

In this study, we successfully synthesized Eu(III)-coordination polymers (Eu-CPs) and utilized them for the highly sensitive detection of DPA (2,6-dipyridine acid). Due to their abundant surface carboxyl and hydroxyl groups, Eu-CPs significantly enhance fluorescence emission in the presence of DPA through the antenna effect. We observed that the competitive binding between DPA and Eu-CPs leads to substantial energy transfer, thereby triggering the characteristic red fluorescence emission of  $\text{Eu}^{3+}$ . Using this method, we achieved a linear detection of DPA concentrations ranging from 0.5 to 80  $\mu\text{M}$ , with a detection limit as low as 15.23 nM and a binding constant of  $3.32 \times 10^3 \text{ M}^{-1}$ . Furthermore, our study demonstrates the potential applications of Eu-CPs in real biological contexts, including the quantitative assessment of bacterial spore numbers and the monitoring of DPA release during spore germination. We validated the accuracy of this method for detecting spore numbers by comparing the results with theoretical values. With this method, we observed that the amount of DPA released from *B. subtilis* spores increased gradually with longer germination times, providing valuable insights for the study of the developmental cycles of microorganisms. Our results emphasize the potential of Eu-CPs to detect DPA, the biomarker of *Bacillus anthracis*, which provides a scientific basis for developing new biological threat detection and prevention strategies. The probe is expected to provide valuable information for studying the growth cycle of microorganisms and preventing the development of harmful pathogens in the future.

**Supplementary Materials:** The following supporting information can be downloaded at: <https://www.mdpi.com/article/10.3390/molecules29174259/s1>, Figure S1: Dynamic light scattering characterization of Eu-CPs; Figure S2: Characterization of Eu-CPs; Figure S3: The stability experiments of the Eu-CPs + DPA; Figure S4: Benesi-Hildebrand plot of Eu-CPs with DPA; Figure S5: The linear relationship between  $I - I_0$  and  $C_{\text{Bacillus subtilis}}$  spores. The concentration of *Bacillus subtilis* activation corresponding to different germination time; Table S1: Comparison of DPA determination between this work and other strategies; Table S2: Different concentrations of *Bacillus subtilis* spores are completely released to obtain the theoretical and actual values of different concentrations of DPA; Table S3: Concentrations of DPA released by *Bacillus subtilis* spores at different germination times. Refs. [40–45] are cited in the Supplementary Materials.

**Author Contributions:** Conceptualization, J.L.; validation Y.L. and C.T.; investigation, J.L. and Y.L.; writing—original draft preparation, J.L. and Y.L.; writing—review and editing, J.L., Y.L., C.T. and L.W.; visualization, Y.L. and C.T.; supervision, C.L., H.Z. and L.Z.; project administration, C.L., C.H. and L.W.; funding acquisition, C.L. and L.W. All authors have read and agreed to the published version of the manuscript.

**Funding:** This work was financially supported by the National Natural Science Foundation of China (NSFC, Grant No. 22074124 and 21976144), a research grant (No. KFKT23006) from Shangqiu Medical College, the Chongqing Talents Program for Outstanding Scientists (No. cstc2021ycjh-bgzxm0179), and Key Research and Development Projects of the Sichuan Science and Technology Department (2023YFS0382).

**Institutional Review Board Statement:** Not applicable.

**Informed Consent Statement:** Not applicable.

**Data Availability Statement:** Data are contained within the article and Supplementary Materials.

**Conflicts of Interest:** The authors declare no conflicts of interest.

#### References

1. Sogues, A.; Fioravanti, A.; Jonckheere, W.; Pardon, E.; Steyaert, J.; Remaut, H. Structure and function of the EA1 surface layer of *Bacillus anthracis*. *Nat. Commun.* **2023**, *14*, 7051. [[CrossRef](#)]

2. Holay, M.; Krishnan, N.; Zhou, J.R.; Duan, Y.O.; Guo, Z.Y.; Gao, W.W.; Fang, R.H.; Zhang, L.F. Single low-dose nanovaccine for long-term protection against anthrax toxins. *Nano Lett.* **2022**, *22*, 9672–9678. [[CrossRef](#)] [[PubMed](#)]
3. Bower, W.A.; Yu, Y.; Person, M.K.; Parker, C.M.; Kennedy, J.L.; Sue, D.; Hesse, E.M.; Cook, R.; Bradley, J.; Bulitta, J.B.; et al. CDC guidelines for the prevention and treatment of anthrax, 2023. *MMWR Recomm Rep* **2023**, *72*, 1–47. [[CrossRef](#)]
4. Wu, J.F.; Chen, P.P.; Chen, J.; Ye, X.X.; Cao, S.R.; Sun, C.Q.; Jin, Y.; Zhang, L.Y.; Du, S.H. Integrated ratiometric fluorescence probe-based acoustofluidic platform for visual detection of anthrax biomarker. *Biosens. Bioelectron.* **2022**, *214*, 114538. [[CrossRef](#)]
5. Hardenbrook, N.J.; Liu, S.H.; Zhou, K.; Ghosal, K.; Zhou, Z.H.; Krantz, B.A. Atomic structures of anthrax toxin protective antigen channels bound to partially unfolded lethal and edema factors. *Nat. Commun.* **2020**, *11*, 840. [[CrossRef](#)] [[PubMed](#)]
6. Mendenhall, M.A.; Liu, S.H.; Portley, M.K.; O'Mard, D.; Fattah, R.; Szabo, R.; Bugge, T.H.; Khillan, J.S.; Leppla, S.H.; Moayeri, M. Anthrax lethal factor cleaves regulatory subunits of phosphoinositide-3 kinase to contribute to toxin lethality. *Nat. Microbiol.* **2020**, *5*, 1464–1471. [[CrossRef](#)] [[PubMed](#)]
7. Yang, N.J.; Isensee, J.; Neel, D.V.; Quadros, A.U.; Zhang, H.-X.B.; Lauzadis, J.; Liu, S.M.; Shiers, S.; Belu, A.; Palan, S.; et al. Anthrax toxins regulate pain signaling and can deliver molecular cargoes into ANTXR2<sup>+</sup> DRG sensory neurons. *Nat. Neurosci.* **2022**, *25*, 168–179. [[CrossRef](#)] [[PubMed](#)]
8. Lu, L.; Shao, X.Y.; Lin, X.X.; Ding, L.H.; Song, B.C.; Sun, J. Tb<sup>3+</sup>-xylene orange complex-based colorimetric and luminometric dual-readout sensing platform for dipicolinic acid and metal ions. *Chin. Chem. Lett.* **2023**, *34*, 107203. [[CrossRef](#)]
9. Cheng, Z.H.; Liu, X.; Zhang, S.Q.; Yang, T.; Chen, M.L.; Wang, J.H. Placeholder strategy with upconversion nanoparticles-eriochrome black T conjugate for a colorimetric assay of an anthrax biomarker. *Anal. Chem.* **2019**, *91*, 12094–12099. [[CrossRef](#)]
10. Wang, D.B.; Cui, M.M.; Li, M.; Zhang, X.E. Biosensors for the detection of Bacillus anthracis. *Acc. Chem. Res.* **2021**, *54*, 4451–4461. [[CrossRef](#)]
11. Zhang, X.R.; Wang, Q.; Sun, X.C.; Asif, M.; Aziz, A.; Zhang, Y.; Dong, C.; Wang, R.B.; Shuang, S.M. Dual fluorophores embedded in zeolitic imidazolate framework-8 for ratiometric fluorescence sensing of a biomarker of anthrax spores. *Chem. Eng. J.* **2024**, *490*, 151582. [[CrossRef](#)]
12. Yu, L.; Feng, L.X.; Xiong, L.; Li, S.; Wang, S.; Wei, Z.Y.; Xiao, Y.X. Portable visual assay of Bacillus anthracis biomarker based on ligand-functionalized dual-emission lanthanide metal-organic frameworks and smartphone-integrated mini-device. *J. Hazard. Mater.* **2022**, *434*, 128914. [[CrossRef](#)] [[PubMed](#)]
13. Pu, S.; Shi, C.T.; Lv, C.Z.; Xu, K.L.; Hou, X.D.; Wu, L. Tb<sup>3+</sup>-based off-on fluorescent platform for multicolor and dosage-sensitive visualization of bacterial spore marker. *Anal. Chem.* **2023**, *95*, 8137–8144. [[CrossRef](#)] [[PubMed](#)]
14. Li, X.Q.; Luo, J.J.; Deng, L.; Ma, F.H.; Yang, M.H. In situ incorporation of fluorophores in zeolitic imidazolate framework-8 (ZIF-8) for ratio-dependent detecting a biomarker of anthrax spores. *Anal. Chem.* **2020**, *92*, 7114–7122. [[CrossRef](#)]
15. Lin, X.D.; Wu, H.T.; Zeng, S.Y.; Peng, T.; Zhang, P.; Wan, X.H.; Lang, Y.H.; Zhang, B.; Jia, Y.W.; Shen, R.; et al. A self-designed device integrated with a Fermat spiral microfluidic chip for ratiometric and automated point-of-care testing of anthrax biomarker in real samples. *Biosens. Bioelectron.* **2023**, *230*, 115283. [[CrossRef](#)]
16. Wu, M.; Jiang, Z.W.; Zhang, P.; Gong, X.; Wang, Y. Energy transfer-based ratiometric fluorescence sensing anthrax biomarkers in bimetallic lanthanide metal-organic frameworks. *Sens. Actuators B* **2023**, *383*, 133596. [[CrossRef](#)]
17. Wang, S.; Xu, J.; Yue, F.Z.; Zhang, L.; Bi, N.; Gou, J.; Li, Y.X.; Huang, Y.Y.; Zhao, T.Q.; Jia, L. Smartphone-assisted mobile fluorescence sensor for self-calibrated detection of anthrax biomarker, Cu<sup>2+</sup>, and cysteine in food analysis. *Food Chem.* **2024**, *451*, 139410. [[CrossRef](#)]
18. Zhang, Y.G.; Wang, X.; Xu, K.X.; Zhai, F.W.; Shu, J.; Tao, Y.; Wang, J.R.; Jiang, L.S.; Yang, L.W.; Wang, Y.X.; et al. Near-unity energy transfer from uranyl to europium in a heterobimetallic organic framework with record-breaking quantum yield. *J. Am. Chem. Soc.* **2023**, *145*, 13161–13168. [[CrossRef](#)]
19. Tong, Y.J.; Gong, X.Y.; Chen, Y.X.; Wu, L.H.; Wang, D.M.; Xu, J.Q.; Gong, Z.J. Promoting photoluminescent sensing performances of lanthanide materials with auxiliary ligands. *Trends Anal. Chem.* **2024**, *171*, 117482. [[CrossRef](#)]
20. Yang, D.F.; Zheng, W.; Huang, P.; Zhang, M.R.; Zhang, W.; Shao, Z.Q.; Zhang, W.; Yi, X.D.; Chen, X.Y. A sandwiched luminescent heterostructure based on lanthanide-doped Gd<sub>2</sub>O<sub>2</sub>S@NaYF<sub>4</sub> core/shell nanocrystals. *Aggregate* **2023**, *4*, e387. [[CrossRef](#)]
21. Zhang, T.T.; Chen, Z.H.; Shi, G.Y.; Zhang, M. Eu<sup>3+</sup>-doped Bovine Serum Albumin-derived Carbon Dots for Ratiometric Fluorescent Detection of Tetracycline. *J. Anal. Test.* **2022**, *6*, 365–373. [[CrossRef](#)]
22. Utochnikova, V.V. The use of luminescent spectroscopy to obtain information about the composition and the structure of lanthanide coordination compounds. *Coord. Chem. Rev.* **2019**, *398*, 113006. [[CrossRef](#)]
23. Du, Y.Y.; Jiang, Y.; Sun, T.Y.; Zhao, J.X.; Huang, B.L.; Peng, D.F.; Wang, F. Mechanically excited multicolor luminescence in lanthanide ions. *Adv. Mater.* **2018**, *31*, 1807062. [[CrossRef](#)] [[PubMed](#)]
24. Paderni, D.; Giorgi, L.; Fusi, V.; Formica, M.; Ambrosi, G.; Micheloni, M. Chemical sensors for rare earth metal ions. *Coord. Chem. Rev.* **2021**, *429*, 213639. [[CrossRef](#)]
25. Koo, T.M.; Ko, M.J.; Park, B.C.; Kim, M.S.; Kim, Y.K. Fluorescent detection of dipicolinic acid as a biomarker in bacterial spores employing terbium ion-coordinated magnetite nanoparticles. *J. Hazard. Mater.* **2021**, *408*, 124870. [[CrossRef](#)]
26. Mohapatro, U.; Mishra, L.; Mishra, M.; Mohapatra, S. Zn-CD@Eu ratiometric fluorescent probe for the detection of dipicolinic acid, uric acid, and ex vivo uric acid imaging. *Anal. Chem.* **2024**, *96*, 8630–8640. [[CrossRef](#)]
27. He, J.H.; Cheng, Y.Y.; Yang, T.; Zou, H.Y.; Huang, C.Z. Functional preserving carbon dots-based fluorescent probe for mercury (II) ions sensing in herbal medicines via coordination and electron transfer. *Anal. Chim. Acta* **2018**, *1035*, 203–210. [[CrossRef](#)]

28. Chen, B.B.; Liu, M.L.; Zhan, L.; Li, C.M.; Huang, C.Z. Terbium(III) modified fluorescent carbon dots for highly selective and sensitive ratiometry of stringent. *Anal. Chem.* **2018**, *90*, 4003–4009. [[CrossRef](#)]
29. Chen, X.B.; Qi, C.-X.; Xu, Y.-B.; Li, H.; Xu, L.; Liu, B. A quantitative ratiometric fluorescent Hddb-based MOF sensor and its on-site detection of the anthrax biomarker 2,6-dipicolinic acid. *J. Mater. Chem. C* **2020**, *8*, 17325–17335. [[CrossRef](#)]
30. Liu, M.L.; Chen, B.B.; He, J.H.; Li, C.M.; Li, Y.F.; Huang, C.Z. Anthrax biomarker: An ultrasensitive fluorescent ratiometry of dipicolinic acid by using terbium(III)-modified carbon dots. *Talanta* **2019**, *191*, 443–448. [[CrossRef](#)]
31. Jiang, L.; Ding, H.; Lu, S.; Geng, T.; Xiao, G.; Zou, B.; Bi, H. Photoactivated fluorescence enhancement in F,N-doped carbon dots with piezochromic behavior. *Angew. Chem. Int. Ed.* **2019**, *59*, 9986–9991. [[CrossRef](#)]
32. Jiang, Z.W.; Zou, Y.C.; Zhao, T.T.; Zhen, S.J.; Li, Y.F.; Huang, C.Z. Controllable synthesis of porphyrin-based 2D lanthanide metal-organic frameworks with thickness- and metal-node-dependent photocatalytic performance. *Angew. Chem. Int. Ed.* **2020**, *59*, 3300–3306. [[CrossRef](#)]
33. Wang, X.; Wang, Y.; Wang, X.Y.; Hu, C.Y.; Wu, X.J.; Guo, W.; Zhen, S.J.; Huang, C.Z.; Li, Y.F. Dual-ligand two-dimensional europium-organic gels nanosheets for ratiometric fluorescence detecting anthrax spore biomarker. *Chem. Eng. J.* **2022**, *435*, 134912. [[CrossRef](#)]
34. Pei, X.J.; Lai, T.C.; Tao, G.Y.; Hong, H.; Liu, F.; Li, N. Ultraspecific multiplexed detection of Low-abundance single-nucleotide variants by combining a masking tactic with fluorescent nanoparticle counting. *Anal. Chem.* **2018**, *90*, 4226–4233. [[CrossRef](#)]
35. Ma, F.; Wang, Q.; Xu, Q.F.; Zhang, C.Y. Self-assembly of superquenched gold nanoparticle nanosensors for lighting up BACE-1 in live cells. *Anal. Chem.* **2021**, *93*, 15124–15132. [[CrossRef](#)] [[PubMed](#)]
36. Huo, P.P.; Li, Z.J.; Yao, R.H.; Deng, Y.H.; Gong, C.C.; Zhang, D.B.; Fan, C.B.; Pu, S.Z. Dual-ligand lanthanide metal-organic framework for ratiometric fluorescence detection of the anthrax biomarker dipicolinic acid. *Spectrochim. Acta Part A* **2022**, *282*, 121700. [[CrossRef](#)] [[PubMed](#)]
37. Zhou, B.; Xiong, Y.F.; Nevo, Y.; Kahan, T.; Yakovian, O.; Alon, S.; Bhattacharya, S.; Rosenshine, I.; Sinai, L.; Ben-Yehuda, S. Dormant bacterial spores encrypt a long-lasting transcriptional program to be executed during revival. *Mol. Cell* **2023**, *83*, 4158–4173.e7. [[CrossRef](#)]
38. Liang, Y.; Yan, Y.; Zou, H.Y.; Yang, T.; Zhen, S.J.; Li, C.M.; Huang, C.Z. Europium coordination polymer particles based electrospun nanofibrous film for point-of-care testing of copper (II) ions. *Talanta* **2021**, *228*, 122270. [[CrossRef](#)]
39. Dey, N.; Biswakarma, D.; Bhattacharya, S. Metal complex as an optical sensing platform for rapid multimodal recognition of a pathogenic biomarker in real-life samples. *ACS Sustainable Chem. Eng.* **2019**, *7*, 569–577. [[CrossRef](#)]
40. Halawa, M.I.; Li, B.S.; Xu, G.B. Novel synthesis of thiolated gold nanoclusters induced by lanthanides for ultrasensitive and luminescent detection of the potential anthrax spores' biomarker. *ACS Appl. Mater. Interfaces* **2020**, *12*, 32888–32897. [[CrossRef](#)]
41. Luo, Y.Q.; Zhang, L.; Zhang, L.Y.; Yu, B.H.; Wang, Y.J.; Zhang, W.B. Multiporous terbium phosphonate coordination polymer microspheres as fluorescent probes for trace anthrax biomarker detection. *ACS Appl. Mater. Interfaces* **2019**, *11*, 15998–16005. [[CrossRef](#)] [[PubMed](#)]
42. Rong, M.C.; Yang, X.H.; Huang, L.Z.; Chi, S.T.; Zhou, Y.B.; Shen, Y.E.; Chen, B.Y.; Deng, X.Z.; Liu, Z.Q. Hydrogen peroxide-assisted ultrasonic synthesis of BCNO QDs for anthrax biomarker detection. *ACS Appl. Mater. Interfaces* **2019**, *11*, 2336–2343. [[CrossRef](#)]
43. Cao, Y.T.; Gong, X.L.; Li, L.; Li, H.H.; Zhang, X.M.; Guo, D.Y.; Wang, F.X.; Pan, Q.H. Xylenol orange-modified CdTe quantum dots as a fluorescent/colorimetric dual-modal probe for anthrax biomarker based on competitive coordination. *Talanta* **2023**, *261*, 124664. [[CrossRef](#)] [[PubMed](#)]
44. Na, M.; Zhang, S.P.; Liu, J.J.; Ma, S.D.; Han, Y.X.; Wang, Y.; He, Y.X.; Chen, H.L.; Chen, X.G. Determination of pathogenic bacteria—Bacillus anthrax spores in environmental samples by ratiometric fluorescence and test paper based on dual-emission fluorescent silicon nanoparticles. *J. Hazard. Mater.* **2020**, *386*, 121956. [[CrossRef](#)] [[PubMed](#)]
45. Shen, M.L.; Liu, B.; Xu, L.; Jiao, H. Ratiometric fluorescence detection of anthrax biomarker 2,6-dipicolinic acid using hetero MOF sensors through ligand regulation. *J. Mater. Chem. C* **2020**, *8*, 4392–4400. [[CrossRef](#)]

**Disclaimer/Publisher's Note:** The statements, opinions and data contained in all publications are solely those of the individual author(s) and contributor(s) and not of MDPI and/or the editor(s). MDPI and/or the editor(s) disclaim responsibility for any injury to people or property resulting from any ideas, methods, instructions or products referred to in the content.